Biophysical Journal
Article

Biophysical Society

Mechanics of inactive swelling and bursting of porate pollen grains

Anže Božič[1] and Antonio Šiber[2,*]
[1]Department of Theoretical Physics, Jožef Stefan Institute, Ljubljana, Slovenia and [2]Institute of Physics, Zagreb, Croatia

ABSTRACT The structure of pollen grains, which is typically characterized by soft apertures in an otherwise stiff exine shell, guides their response to changes in the humidity of the environment. These changes can lead to desiccation of the grain and its infolding but also to excessive swelling of the grain and even its bursting. Here we use an elastic model to explore the mechanics of pollen grain swelling and the role of soft, circular apertures (pores) in this process. Small, circular apertures typically occur in airborne and allergenic pollen grains so that the bursting of such grains is important in the context of human health. We identify and quantify a mechanical weakness of the pores, which are prone to rapid inflation when the grain swells to a critical extent. The inflation occurs as a sudden transition and may induce bursting of the grain and release of its content. This process crucially depends on the size of the pores and their softness. Our results provide insight into the inactive part of the mechanical response of pollen grains to hydration when they land on a stigma as well as bursting of airborne pollen grains during changes in air humidity.

SIGNIFICANCE Pollen grains undergo significant changes in their water content during transfer from the anther to the stigma. Airborne pollen grains are particularly sensitive to atmospheric changes. In a humid environment, they swell and may rupture, releasing their cytoplasmic content, which may provoke allergic reactions in sensitive individuals. The mechanics of this process are poorly understood, and it is not known why pollen grains of some species are more resistant than others. We show that grain bursting critically depends on the presence of pores, soft spots in the grain wall. The occurrence of bursting is determined by the interplay between pore softness and pore size.

INTRODUCTION

The ability of pollen grains to adapt to physical and biochemical changes in their environment is essential for their survival. When pollen grains leave the environment of the anther, they start to lose water, and this process activates a variety of protective mechanisms (1,2). Upon landing on a stigma, they take in exudate from its cells, swell, and eventually germinate, forming a pollen tube through which they fertilize the flower (3,4). Although growth of the pollen tube is an active response of the pollen grain, which requires coherent mobilization of numerous cellular mechanisms, precise regulation of osmotic forces (5), and deposition of biopolymers in the growing tube (6,7), the mechanical response of pollen grains to changes in their water content is, to a large degree, inactive and a consequence of their mechanical constitution (8–10). This mechanical makeup has its drawbacks, however, because it can induce an extreme response of the grains in a non-reproductive context. When the environmental conditions change suddenly (e.g., when the relative humidity of the atmosphere increases significantly), such a response may lead to the bursting of pollen grains (9,11). This typically occurs in windborne pollen grains when they have been lifted up from the anthers into the atmosphere. For instance, the concentration of grass allergens in the non-pollen-containing fraction of ambient air has been shown to correlate with air humidity (12), which, in turn, is related to the bursting of the pollen grains (11).

Understanding pollen bursting is important not only from the perspective of grain viability and plant fertilization but also in the context of human health because ruptured airborne grains can release respirable fragments that can provoke allergic reactions in exposed sensitive individuals (13–15). In regions of intense agricultural activity, for example, some monocultures—particularly those pollinated by wind—can produce huge quantities of pollen prone to bursting (16), and similar problems occur with urban

Submitted September 6, 2021, and accepted for publication January 21, 2022.

*Correspondence: asiber@ifs.hr

Editor: Padmini Rangamani.
https://doi.org/10.1016/j.bpj.2022.01.019

horticultural planning (13,17). Although grain bursting and the consequential release of its content is not characteristic only of allergenic pollen, being a general feature of pollen that hydrates rapidly (9), it is a necessary process for realization of the allergenic potential of a species (11,16). Pollen allergens released in the atmosphere when the grains burst can affect human health for a long time, even when the pollen grains are destroyed and no longer viable (15). The grains, and in particular the cytoplasmic fragments they release when they burst, can also act as effective nucleation sites for cloud condensation (18–20), which can influence precipitation (21). Bursting of pollen grains in the atmosphere is thus relevant medically and meteorologically. Last, the spatial distribution of stresses effected by the inactive mechanical response of the grain could tag the site where the pollen tube originates and trigger and guide the active mechanisms for its growth (5,22). These examples highlight the importance of a quantitative description of pollen grain swelling and bursting to understand a wide range of phenomena in different environments and on very different scales.

Any model constructed to represent the influence of changing water content on pollen grain volume and shape needs to account for the inhomogeneities in the grain wall. Pollen grain walls of an overwhelming majority of gymnosperm and angiosperm species have discernible regions called apertures, which are known to differ in chemical and structural composition from the rest of the wall (3). The larger part of the pollen shell contains a rigid layer, called the exine, which is mostly made of sporopollenin. The apertures are regions in the shell where the exine layer is thinned or entirely absent and mostly consist of cellulose and pectin, making them typically (much) softer than the exine (23,24). Apertures thus act as flexible regions in an otherwise stiff pollen shell. Because the exchange of water between the pollen grain and its surroundings takes place mostly through the apertures (1,25), their closure and concomitant infolding of the pollen grain provides a mechanical response that prevents further desiccation and destruction of the grain. It has been shown recently that the success of this process requires a tuned mechanical flexibility of the grain wall so that closing of the apertures also pulls in the hard, exine parts of the grain (8,10) without inducing rupture in the wall material.

Much less is known about the influence of different features of pollen morphology on the swelling and bursting of the grains, which can happen by rupture of the apertures or the exine (9). Our aim is to investigate how pollen grains passively respond to (re)hydration and what role apertures play in this process. We focus on pollen grains with circular apertures called pores (3), which is the dominant type of pollen of anemophilous (wind-pollinated) plants (26). Experiments have shown that pores mechanically respond to hydration (3,9,25), but a theoretical description of this process it still lacking. To describe the swelling and possible rupture of porate pollen grains, we formulate an elastic model of the grain akin to one established previously to describe the shape changes in drying grains (10). We examine how the presence of pores influences the swelling of pollen grains as their volume increases because of the influx of fluid from the environment. The increase in grain volume is shown to cause rapid inflation of the pores, which results in huge strain on the pore material. We explore how the size, number, and distribution of pores influence deformation of the pollen grain and its resistance to pore inflation and bursting. Our results provide quantitative theoretical insight into the inactive mechanisms behind the bursting of pollen grains, and the model we use can be generalized to study the swelling of other types of aperturate pollen grains as well.

MATERIALS AND METHODS

Elastic model of the pollen grain

Construction of the elastic triangular mesh of the pollen grain and the elastic energy functional assigned to it closely follows the method used previously by Božič and Šiber (10). We assume that there exists an unstrained state of the pollen grain of volume V_0, which is perfectly spherical and represents the reference, equilibrium state of the problem. The pollen grain can desiccate, which leads to a reduction of its volume $V<V_0$, or it can further hydrate, leading to an increase in its volume $V>V_0$.

Elastic energy of the grain

The elastic energy of the pollen wall can be formulated so that the microscopic energies effectively reside in the edges of the mesh:

$$E = \sum_i \frac{k_i}{2}(l_i - l_{i,0})^2 + \sum_i \rho_i\left[1 - \cos\left(\phi_i - \phi_{i,0}\right)\right]. \qquad (1)$$

The first and the second term in Eq. (1) are the stretching and the bending energy, respectively. The mesh (triangle) edges i have lengths l_i, which, in general, differ from their equilibrium lengths $l_{i,0}$ in the unstrained state. The stretching energy of an edge is proportional to the square of its extension $\Delta l = l_i - l_{i,0}$; i.e., each edge i acts as a Hookean spring with a spring constant k_i. The bending energy associated with the i-th edge can be expressed via the angles φ_i between the two triangle faces that share the edge. The bending energy depends on the difference between the actual and the equilibrium angles (φ_i and $\varphi_{i,0}$, respectively).

The bending and stretching elastic constants of an edge can take on two different values, depending on whether the edge belongs to the exine or to the pore region of the grain wall, because the two regions have different elastic properties: for edges in the exine region, $k_i = k_{ex}$ and $\rho_i = \rho_{ex}$, and for edges in the pore region, $k_i = k_p$ and $\rho_i = \rho_p$. The values of the elastic constants in the pore region are scaled by a softness parameter $f<1$ (8) so that $k_p = fk_{ex}$ and $\rho_p = f\rho_{ex}$. Edges that have bounding vertices in different regions, one in the exine and the other in the pore region, are assigned a stretching constant of $k_i = (k_{ex} + k_p)/2$. Similarly, when the geometrical centers of two faces sharing an edge are in different regions, the edge is assigned a bending constant of $\rho_i = (\rho_{ex} + \rho_p)/2$.

We also introduce a dimensionless quantity $\overline{\gamma}$, which signifies the relative contributions of the bending and stretching energies and is defined as

$$\overline{\gamma} \equiv \frac{k_{ex}R_0^2}{\rho_{ex}} = \frac{k_pR_0^2}{\rho_p}. \qquad (2)$$

This quantity, defined through microscopic elastic constants and used already in our previous work (10), differs from the Föppl-von Kármán number of the exine (or pore) sheet defined through continuum elastic constants by a factor on the order of unity. This is a consequence of the discrete form of bending energy we use (second term in Eq. (1)), whose continuum limit depends on the topology of the shape (27–29). For a more detailed discussion of the our model, we refer the reader to our previous work (10).

Mesh triangulation

This mesh obtained from the marching triangulation (30) is preconditioned so that the local elastic responses in the mesh without the pores ($f = 1$) are as uniform as possible. When the mesh is optimized, the resulting edge lengths and angles are defined to be the equilibrium values of the edge lengths and angles, and this produces the set of constants $l_{i,0}$ and $\varphi_{i,0}$ in the energy functional in Eq. (1). When such a mesh is inflated for a grain without pores, the strains are checked to be nearly uniform and isotropic throughout the mesh, as they must be according to Eq. (5). Indeed, they differ from the analytical prediction by at most $\sim 1\%$. For the results shown in this work, the stress- and strain-free state is a spherical shell of radius $R_0 = 38.4a$, where a is the mean length of the mesh edge. The mesh has $\mathcal{V} = 21644$ vertices, $\mathcal{E} = 64926$ edges, and $\mathcal{F} = 43284$ faces, and $\mathcal{V} - \mathcal{E} + \mathcal{F} = 2$, as it must be according to the Euler formula for polyhedra (31).

Minimization procedure

The energy functional in Eq. (1) is minimized with respect to the coordinates of the mesh vertices using the conjugate gradient method of Hager and Zhang (32). The volume of the mesh is constrained by adding an extra term to the energy functional of the form

$$E_{\text{penal}} = K_V (V - V_0)^2, \tag{3}$$

where K_V is the volume penalization constant. The constant must be chosen with care because values that are too small do not constrain the volume to a sufficient precision, whereas values that are too large may result in problems with the convergence of the minimization. The appropriate value of the constant K_V can be determined by a sequence of minimizations in which the constant is multiplied by a factor of $F>1$ in each step, as described, for instance, by Šiber (33). When the minimization is finished, the penalty energy, because of the constraint in Eq. (3), must be a negligible percentage of the total elastic energy of the mesh. When the minimal shape for a given relative additional volume $v \equiv V/V_0 - 1$ is obtained, all mesh vertices are randomly jittered, i.e. displaced typically between 0 and 0.1a in random directions, and the minimization is repeated. The volume is then increased or decreased, depending on whether the minimization proceeds along the forward or the backward path, respectively.

Strains in the pollen grain

To effectively measure the magnitude of the strains in the pollen grain, we define a suitably averaged measure of strain ε_v in each vertex v of the mesh. This quantity is obtained from the area A_v of all triangles sharing the vertex v,

$$\varepsilon_v = \sqrt{\frac{A_v}{A_{v,0}}} - 1, \tag{4}$$

where $A_{v,0}$ is the area of all triangles around the vertex v in the strain-free state of the mesh. In the case of small deformations, the scalar ε_v in Eq. (4) can be thought of as the average value of the magnitudes of principal strains. The averaged measure of strain in the entire pore $\bar{\varepsilon}_p$ is then calculated by summing the quantities ε_v over all vertices v that belong to the pore region and dividing the result by the total number of vertices in the pore.

RESULTS

Mechanical properties of porate pollen grains

Pollen species with porate grains are ubiquitous, particularly in anemophilous plants (26), and represent a large proportion of allergenic pollen species (15). Their pollen grains can have different shapes with a more or less pronounced asphericity. Here we assume that the grains are perfectly spherical in the equilibrium state (thus neglecting any initial asphericity) with an equilibrium radius R_0. Although the model we use allows different equilibrium grain shapes, the assumption of spherical grains reduces the number of parameters of the model and allows simpler identification and classification of the important features of grain swelling. The porate pollen grains can be further characterized by the number N of identical (circular) pores they contain, their distribution, and the angular span of each pore θ_0 (see the examples in Fig. 1).

Inaperturate pollen—pollen without any apertures—with $N = 0$ can be considered an extension of the geometric class of porate pollen and represents, at least on the level of our model, mechanically the simplest case of a porate pollen grain. The genus *Populus*, for instance, contains many anemophilous species with inaperturate pollen, some of which are also moderately allergenic (e.g., *Populus alba*) (34). Monoporate pollen ($N = 1$) is characteristic of most of the species in the Poaceae family (grasses) (3), to which some of the most allergenic anemophilous plant species belong (e.g., *Phleum pratense*) (15). Diporate pollen grains ($N = 2$), with the two pores situated diametrically on the equator of the grain, can be found, for instance, in *Morus alba*, although the grains of this species can also have three and four pores. Triporate pollen ($N = 3$), with the three pores arranged equidistantly on the equator of the grain, are typical for *Ambrosia artemisiifolia* and the majority of species in the Betulaceae family, although some Betulaceae species also have five ($N = 5$) equatorially situated pores (e.g., *Alnus glutinosa*). Lastly, *Amaranthus* species are typically pantoporate—they have many pores ($N \approx 20$ to 60) distributed nearly uniformly on the grain surface (35). The opening angles of the pores can be estimated from microscopic images of hydrated grains (3) and in general depend on the species, but they are typically about $\theta_0 \sim 0.1$ (36,37), such as in *Betula pendula* (Fig. 1 *c*) and *Ulmus parvifolia* (3). In two more extreme examples, the pore angles of *Stellaria aquatica* (Fig. 1 *e*) and *Zea mays* are about $\theta_0 \approx 0.18$ (38) and $\theta_0 \approx 0.05$ to 0.07 (39), respectively.

The Föppl-von Kármán number, $\overline{\gamma}$, of pollen grains is typically in the range of $\overline{\gamma} \sim 10^3$ to 10^4 (10). The softness parameter of the pores has been estimated in our previous study to be in the range of $f \sim 0.01$ to 0.1 (10). It is a relatively simple feat to measure the volume of a pollen grain as it hydrates by measuring its dimensions (40,41). This is why we perform elastic calculations at a given volume of the

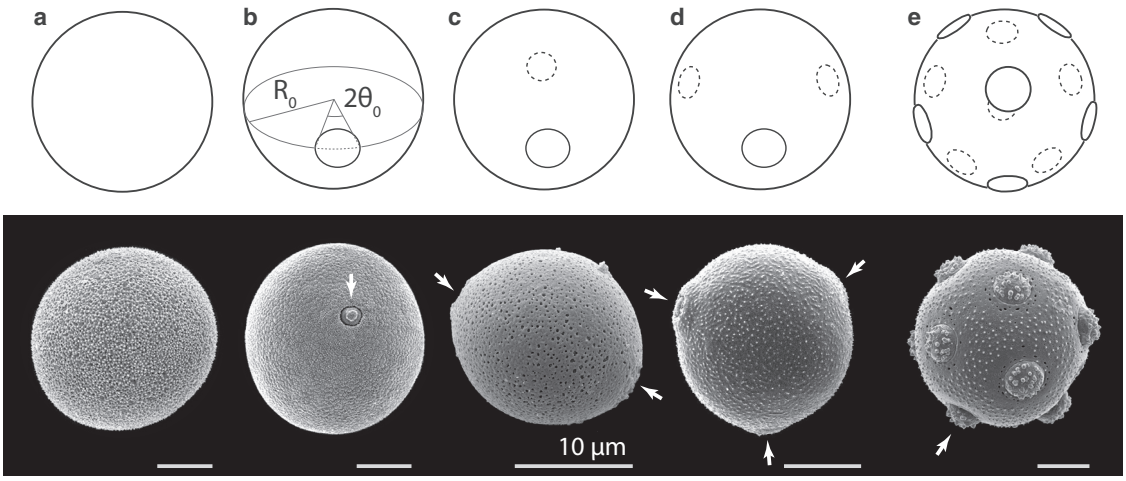

FIGURE 1 Porate pollen. Classes of porate pollen considered in this study. (*a–e*) inaperturate ($N = 0$) (*a*), monoporate ($N = 1$) (*b*), diporate ($N = 2$) (*c*), triporate ($N = 3$) (*d*), and pantoporate ($N \sim 10$; in this case, $N = 12$) (*e*). (*b*) also illustrates the parameters of the pore geometry—its equilibrium, unstrained radius R_0, and the pore opening angle θ_0. Pore size in each schematic porate pollen is $\theta_0 = 0.2$. The bottom part of each panel shows a scanning electron microscopy image of a pollen grain representative of the class: (*a*) *P. alba*, (*b*) *P. pratense*, (*c*) *Besleria solanoides*, (*d*) *B. pendula*, and (*e*) *S. aquatica*. The scale bars represent 10 μm, and the arrows point to the grain pores. In (*e*), only one of the 12 pores is indicated. Pollen images are reprinted with permission from the Society for the Promotion of Palynological Research in Austria; images courtesy of PalDat (2000 onward, www.paldat.org).

grain, treating it as a mechanical constraint. The minimization of the elastic energy yields simultaneously the grain shape and the distribution of elastic strains in the grain wall (in the pore and in the exine regions).

Swelling of inaperturate pollen grains

As a pollen grain hydrates, its volume increases, and its shape changes depending on its elasticity and the distribution, size, and shape of the pores. It is instructive to first consider the swelling of an inaperturate pollen grain—a perfectly homogeneous and spherical elastic shell of radius R_0 enclosing a volume V_0. Such a shell responds to an increase in its interior volume V by an isotropic increase in its radius R. The influence of pores on pollen grain deformation can then be compared with this idealized case, which approximates a perfectly spherical inaperturate pollen grain ($N = 0$; Fig. 1 *a*).

The extensional strains ε_0 in a homogeneous spherical shell are the same everywhere and can be obtained from

$$\varepsilon_0 = \frac{\Delta l}{l_0} = \frac{\Delta R}{R_0} = \left(1 + \frac{\Delta V}{V_0}\right)^{1/3} - 1, \qquad (5)$$

where $\Delta l/l_0$ represents the relative increase in the arbitrarily oriented infinitesimal lengths in the surface of the shell as they extend from l_0 in the initial state to $l_0 + \Delta l$ in the swollen state (42). Similarly, ΔR denotes the corresponding increase in the radius of the shell when its volume increases by $\Delta V = V - V_0$ (43). For small values of relative additional volume, Eq. (5) reduces to $\varepsilon_0 = v/3$. This can be applied to the case of inaperturate pollen; when the strain in the exine exceeds a critical value (i.e., when the additional volume v becomes large enough), the grain wall will break. For example, if the rupture strain of the exine is 10%, then the inaperturate grain can increase its volume by 30% before it ruptures. This estimate is, in fact, of the correct order of magnitude; a rupture strain of $\sim 20\%$ has been measured in inaperturate pollen of *Cryptomeria japonica* (44), and similar values are found in experiments on exine deformation and rupture (45). The estimate effectively presumes that the material deforms elastically all the way until fracture. This appears to be a good approximation for exine and cellulose films (45–47).

Swelling of monoporate pollen grains

If there are pores in the pollen grain, they can relieve some of the swelling strain and, thus, change the nature of the grain fracture. We first investigate how the presence of a single soft pore ($N = 1$; Fig. 1 *b*) influences the swelling of pollen grains. Fig. 2 illustrates and quantifies this process of an increase in the volume of a pollen grain with $f = 0.02$, $\theta_0 = 0.15$, and $\overline{\gamma} = 10^4$. Fig. 2 *a* shows the effect of increasing volume on the pore strain, which is averaged over the entire pore surface, $\overline{\varepsilon_p}$, and scaled by the strain, which would be characteristic for an inaperturate grain of the same volume, ε_0 (i.e., when $f = 1$ or $N = 0$; Eq. (5)). The most notable feature of hydration of the monoporate grain is the sudden jump in pore strain, which, for this particular choice of elastic parameters, occurs at a relative additional volume of $v_c = 0.263$. At this point, the average scaled pore strain increases from $\overline{\varepsilon_p}/\varepsilon_0 \approx 15$ to $\overline{\varepsilon_p}/\varepsilon_0 \approx 55$. An even more drastic increase is observed in the maximum scaled pore strain, which is located at the outermost point of the pore and increases from $\varepsilon_{p;\max}/\varepsilon_0 \approx 29$ to

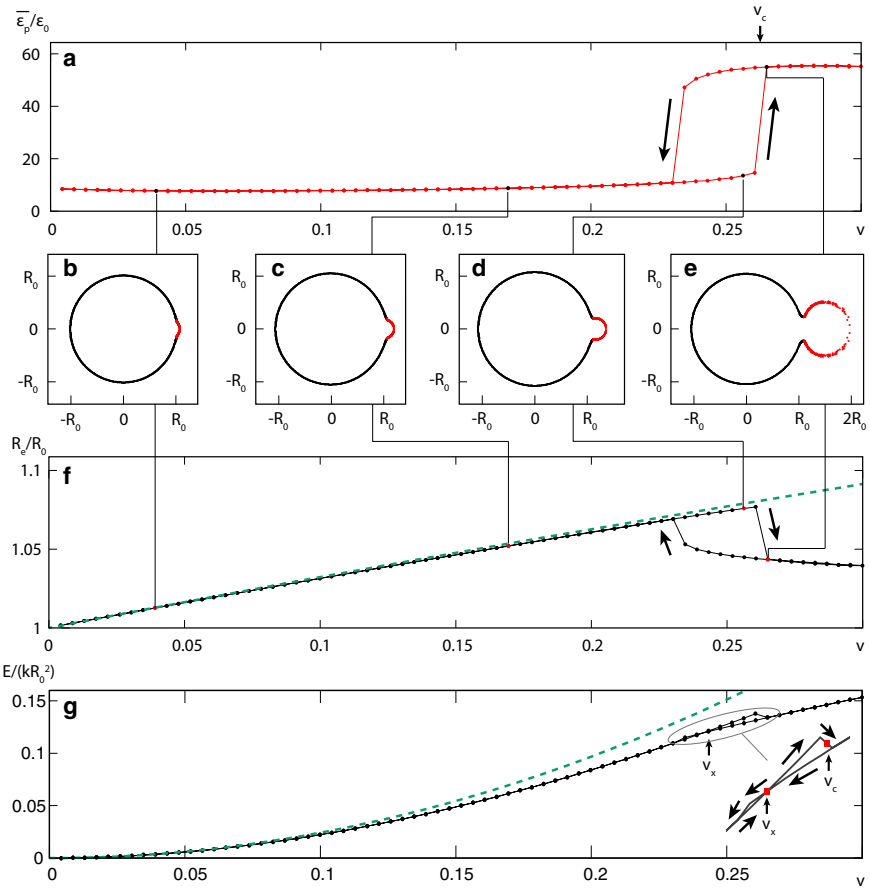

FIGURE 2 Swelling of a monoporate pollen grain. (*a*) Pore strain averaged over the pore area $\overline{\varepsilon}_p$ and scaled by strain in a homogeneous (inaperturate) grain ε_0 (given by Eq. (5)) as a function of relative additional volume $v = V/V_0 - 1$. (*b–e*) Cross-sectional projections of the mesh points of the model for $v = 0.04$, 0.17, 0.256, and 0.265. In these panels, the pore and exine materials are denoted by red and black dots, respectively. The procedure used to generate these projections is described in the supporting material. (*f*) Dimension of the bounding box of the exine part of the pollen grain in the direction perpendicular to the axis connecting the centers of the grain and the pore (i.e., along the ordinate axis in *b–e*). The dashed line indicates the increase in radius that would occur in an inaperturate, homogeneous grain, $R/R_0 = (1+v)^{1/3}$. (*g*) Total energy of the pollen grain mesh scaled by kR_0^2 (black line with symbols). The dashed line indicates the continuum limit of the stretching energy in the elastic discrete model of an inaperturate, homogeneous grain, $E_s/kR_0^2 = 4\pi/(3\sqrt{3})\,v^2$. The inset shows the magnified region of v where the hysteresis occurs. Elastic parameters of the pollen grain are $f = 0.02$, $\theta_0 = 0.15$, and $\overline{\gamma} = 10^4$ throughout. To see this figure in color, go online.

$\varepsilon_{p;\max}/\varepsilon_0 \approx 196$. Note here that this is a scaled quantity, where $\varepsilon_0 \approx v/3$ is about 0.09 at $v_c = 0.263$, meaning that the maximum pore strain jumps from about $\varepsilon_{p;\max} \approx 2.6$ just before the transition to about $\varepsilon_{p;\max} \approx 18$ after the transition. The sudden transition observed in the pore strain exhibits hysteresis, as seen by the non-equivalence of the forward and backward minimization paths of gradual increase and decrease of internal volume, respectively (marked by arrows in Fig. 2 *a*).

Fig. 2, *b–e*, shows the cross-sectional projections of the triangular mesh of the model grain at different relative additional volumes, $v = 0.04$, 0.17, and 0.256 (just before the transition), and 0.265 (just after the transition). The sudden inflation of the pore (shown in red) at the critical volume v_c is very pronounced. The mean radius of the exine region of the pollen grain (shown in black) increases until the transition point at v_c and suddenly decreases afterward. This change is quantified in Fig. 2 *f*, which shows the effective radius of the pollen grain in the direction perpendicular to the line joining the centers of the grain and the pore (ordinate axis in Fig. 2, *b–e*). The dashed line shows the increase in the exine radius, which would be expected in the case of an inaperturate grain, $R_e/R_0 = (1+v)^{1/3}$. The mean radius of the exine region follows this dependence quite closely for small v, but the increase slows down as the grain volume approaches v_c and the exine abruptly deflates at the critical volume, compensating in this way for the sudden inflation of the pore.

The inflation of the pore can also be traced in the elastic energy of the pollen grain, as shown in Fig. 2 *g*, where a sudden drop in energy is observed at v_c. This calculation also reveals two different energy behaviors that represent two different states of the system. In one of them, the pore still encloses a fairly small volume and has not yet bulged out, whereas in the other, the pore has bulged out and the exine has relaxed. Intriguingly, the two energy behaviors cross at volume $v_x < v_c$, which suggests that the true energy minimum of the system cannot be reached for all volumes; i.e., the pore needs to sufficiently deform before it can bulge out and transition to a lower-energy state. This is illustrated in the inset of Fig. 2 *g*, which shows the magnified portion of the forward and backward minimization paths near the intersection of the two energy curves. The inflation of the pore during grain swelling results in lower elastic energies of the grain compared with an inaperturate grain of the same volume. The stretching elastic energy of the latter, $E_s/kR_0^2 = 4\pi/(3\sqrt{3})\,v^2$, which is the analytical limit of the stretching energy encompassed by the microscopic numerical model in such a situation, is shown by a dashed line.

Mechanics of the bursting transition

When the increase in volume of a monoporate pollen grain reaches a critical relative additional volume v_c, the strains in the pore increase manyfold, which can cause it to burst. It is therefore appropriate to call the sudden inflation a bursting transition. Bursting of a monoporate grain can be viewed as a transition of the pore through a state when it is maximally curved—this is the state when the inflated pore resembles a hemisphere (Fig. 2 *d*). Up to that point, the pore can resist the internal pressure mainly by increasing its curvature because the reaction force of the inflated pore is proportional to the inverse radius of curvature (see the discussion in the supporting material). Past that point, however, the pore radius must increase because of the geometry of the problem, and to resist the additional pressure, the tension in the pore material must increase to resist the same pressure at a larger pore radius. This leads to sudden inflation of the pore.

The physical mechanism behind the bursting transition can be quantified by equating the normal reaction forces of the exine and the pore at the poles because they must resist the same internal pressure in the grain (42,43). When this analysis is performed for the maximal curvature of the pore (i.e., when the pore attains a (nearly) hemispherical shape), one obtains the following equation for the critical relative additional volume of the grain at which the sudden pore inflation occurs (see the supporting material for details of the derivation):

$$v_c = \left(\frac{\theta_0 - f}{\theta_0 - f\pi/2}\right)^3 \left(1 + \frac{\theta_0^3}{2}\right) - 1. \tag{6}$$

The relation was derived assuming a negligible influence of the bending energies on the transition, which can be seen by the lack of dependence of v_c on $\overline{\gamma}$. When $f/\theta_0 \ll 1$ and $\theta_0 \ll 1$, conditions likely to be fulfilled by most pollen grains, the expression for the critical volume reduces to

$$v_c \approx 1.71 \frac{f}{\theta_0}. \tag{7}$$

Although Eqs. (6) and (7) give only rough estimates of the critical volume of the bursting transition, they are important because they demonstrate that, for the mechanical parameters typical for pollen grains, the critical volume for bursting should primarily depend on the ratio of the softness of the pore (compared with the exine) and the pore size.

To fully inflate (and eventually burst), the pore must pass through a hemispherical state. However, even when the pore has not yet sufficiently inflated to reach the hemispherical shape, there might exist inflated states of the pore (i.e., pores larger than a hemisphere) with lower elastic energies. Such states are, however, not geometrically accessible because they can be reached only after the pore passes through the hemispherical state. In this case, the hemispherical state of the pore represents a geometrical hindrance or a bottleneck and acts as an effective energy barrier. This effect is somewhat similar to the "blowout" or bursting instability observed in inflation of flat circular membranes (48,49). In our numerical simulations, the energy barrier can be most easily detected by the hysteretic nature of the minimization, as demonstrated in Fig. 2. It is also worth mentioning here that the analogy between pore inflation and "blowing a balloon confined in a rigid box" has been noted previously by Matamoro-Vidal et al. (9) in discussions of experiments on pollen swelling.

With this insight, we can now rationalize the two characteristic volumes v_c and v_x, which were detected in the dependence of the elastic energy of the pollen grain on its volume (Fig. 2 *g*). The first of the characteristic volumes, v_x, is the relative additional volume at which the state with the inflated pore (larger than a hemisphere) becomes advantageous with respect to the total elastic energy. The second characteristic volume, v_c, is the critical relative additional volume when the internal pressure becomes large enough to surmount the energy barrier of the hemispherical shape and allows the pore to attain the inflated shape. This critical volume, which can be identified in the forward minimization procedure, is relevant for hydration of pollen grains. The analytical considerations given by Eq. (6) also pertain to this volume. The volume where the energy curves cross (v_x) can be detected by combining the results of the forward and backward minimization procedures (see Fig. 2 *g*). Thus, at $v = v_x$, there exist two different states of the grain with the same energy (shown in an example in Fig. 3). In one of those states, denoted by 1 in Fig. 3, the pore has not yet reached the critical, hemispherical shape, whereas in the other state, denoted by 2 in Fig. 3, the pore has inflated. These two shapes are obtained in the forward and backward minimization paths at $v = v_x$, respectively.

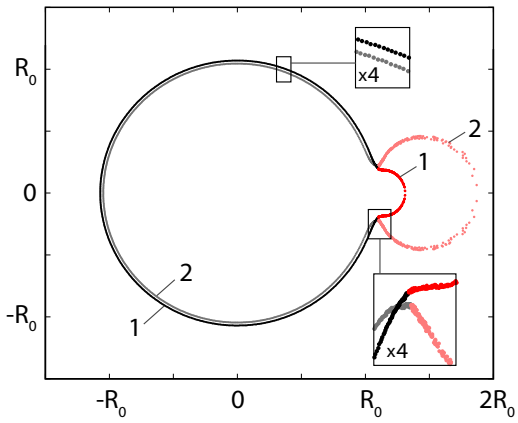

FIGURE 3 Two states of the grain with the same elastic energy. Cross-sectional projections of two states of the grain (shown in light and dark shades, respectively) with the same elastic energy at $v = v_x = 0.241$ (as marked in Fig. 2 *g*). Insets show the magnified regions of the grain cross-sections. Elastic parameters of the grain are $f = 0.02$, $\theta_0 = 0.15$, and $\overline{\gamma} = 10^4$. To see this figure in color, go online.

Bursting transition and pore size and softness

To further corroborate the physical interpretation of the volumes v_c and v_x, we show in Fig. 4 how these volumes change with the pore opening angle θ_0 and different values of the pore softness parameter f. In particular, we examine the range of θ_0 relevant for porate pollen grains; see the examples in Fig. 1 for an illustration of the different pore sizes. One can observe that the analytical prediction of Eq. (6) becomes progressively worse as f increases. This is to be expected because the equation stops making sense as f becomes comparable to θ_0, which can happen for small pore opening angles or sufficiently large f, and it has a divergence at $f = 2\theta_0/\pi$. Nevertheless, the simple physical reasoning behind Eq. (6) explains the salient features of the numerical results in the range of parameters f and θ_0 typical for monoporate pollen grains. It is worth reiterating that the critical volume at which the pore inflates and bursts does not depend on the elasticity of the exine or the pore alone but on the softness of the pore compared with the exine (softness parameter f). When the pores are sufficiently large, the energy barrier for the pore inflation disappears, and the two characteristic volumes become identical: $v_x = v_c$. The rather rapid inflation of the pore still persists, although it now becomes a continuous phenomenon. Furthermore, the hysteresis of the numerical calculation disappears, which indicates disappearance of the energy barrier for the bursting transition; for $f = 0.02$, for instance, this happens for opening angles larger than $\theta_0 \approx 0.2$ (Fig. 4 *b*). The increase in strains in the pore during the bursting transition becomes smaller as the pore gets larger.

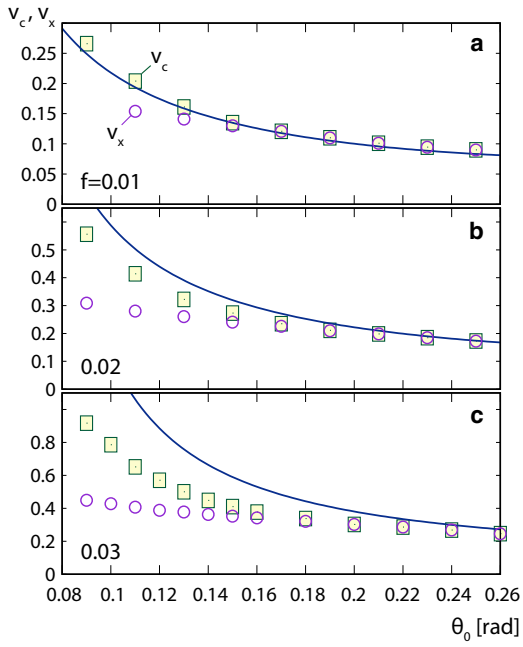

FIGURE 4 Critical volumes and pore softness. Critical relative additional volume v_c, at which a pore rapidly inflates (squares), and relative additional volume v_x, at which the state with the inflated pore has a lower total energy (circles), as a function of the pore opening angle θ_0 for monoporate grains with $\overline{\gamma} = 10^4$. Results are shown for three different pore softness parameters: (*a*) $f = 0.01$, (*b*) 0.02, and (*c*) 0.03. Full lines show the prediction of Eq. (6). To see this figure in color, go online.

Bursting of pollen grains with two or more pores

Swelling of monoporate grain eventually leads to inflation and bursting of the pore, unlike in the case of inaperturate pollen, where swelling causes fracture of the exine when the strains become too large. Pore size and softness limit the amount of swelling a grain can tolerate before it ruptures. Simple analytical considerations of the bursting transition suggest that the critical volume v_c is not significantly modified by the number of pores in the grain as long as these are sufficiently small. More precisely, as long as $N\theta_0^3/2 \ll 1$, the critical volume of a grain with N pores,

$$v_c = \left(\frac{\theta_0 - f}{\theta_0 - f\pi/2}\right)^3 \left(1 + N\frac{\theta_0^3}{2}\right) - 1, \qquad (8)$$

should essentially remain the same as in the case of monoporate grains. One could argue that the final state of the inflated pores is now less strained because the additional volume is distributed among several pores. However, numerical calculations indicate that inflation past the critical point is always asymmetric. Even the slightest difference between the pores leads to a situation where one of the pores inflates much more than the rest and bursts. This is shown in Fig. 5 for a pantoporate pollen grain with $N = 12$ pores, where a single pore suddenly inflates after the bursting transition, whereas the other 11 pores deflate. The surface of the pollen grain is colored in accordance with the local strain in the grain so that the darkest blue and the brightest yellow represent the smallest and largest values of averaged strain when it is larger than it would be in an inaperturate grain with the same volume. One can observe that regions with an increased strain compared with an inaperturate grain are restricted exclusively to the pores. On the other hand, the strains in the exine are quite uniform (gray regions) and reach only about 71% of the value that they would in an inaperturate grain (see the inset in Fig. 5). These two observations demonstrate that the pores act to relieve some of the strain on the exine, the more so the smaller the ratio f/θ_0, i.e. the softer and larger the pores are (see also the supporting material).

In Fig. 6, we show the bursting volumes of pollen grains with $f = 0.02$ and $N = 2$, 3, and 4 pores arranged equidistantly along the equator of the grain as well as of a pantoporate grain with $N = 12$ pores arranged on the vertices of an icosahedron. Diporate pollen grains with two diametrically positioned pores behave essentially the same as monoporate grains (Fig. 6 *a*); their critical volumes differ very little, and the two pores in diporate grains do not interact in the relatively wide range of pore opening angles considered. However, as the number of pores increases, critical volumes of

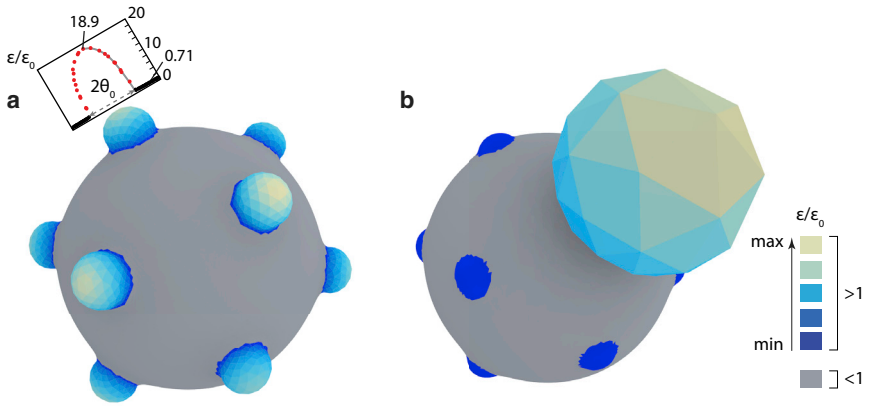

FIGURE 5 Pore inflation in pantoporate pollen grain. Pantoporate grain with $N = 12$ pores arranged around icosahedron vertices (*a*) right before the bursting transition ($v_c = 0.389$) and (*b*) just after it ($v_c = 0.402$). The large sphere-like bulge in the upper right portion of (*b*) is the inflated pore. Mesh triangles are colored in accordance with the scaled local strain $\varepsilon/\varepsilon_0$. The parts of the grain where the strains are smaller than in the inaperturate case ($\varepsilon/\varepsilon_0<1$) are colored in gray. The parts where $\varepsilon/\varepsilon_0>1$ are colored using the color scale shown in the legend so that blue and yellow correspond to smallest and largest values of $\varepsilon/\varepsilon_0>1$, respectively. The maximal relative strains in the grains in (*a*) and (*b*) are $\varepsilon/\varepsilon_0 = 18.9$ and 178, respectively; in both cases, corresponding to the brightest yellow. The inset in (*a*) shows the cross-sectional profile of the relative strains in the plane that contains the maximally strained point of the pore (its pole) and the grain center. The points corresponding to the pore and the exine are indicated by red and black circles, respectively. The x axis in this diagram is the angular coordinate of the mesh points in the chosen cross-section and is appropriately scaled to match the 3D representation. Elastic parameters of the pollen grain are $f = 0.02$, $\theta_0 = 0.15$, and $\overline{\gamma} = 10^4$. To see this figure in color, go online.

porate grains begin to deviate from the values obtained in monoporate grains, which can be interpreted as a consequence of an effective elastic interaction between the pores. This effect occurs only for sufficiently large pore opening angles, when the pores themselves become large and move closer to each other. The region of θ_0 where this effect becomes noticeable is shown by thick light-blue lines on x axes in Fig. 6, *b–d*. As the number of pores in pollen grains increases, the range of pore sizes where pores interact with each other increases as well, and the pores start to interact at ever smaller values of θ_0. The effect of the pore-pore interaction cannot be accounted for solely by the volume they share, as predicted by Eq. (8), because this provides only a barely visible correction for $N = 3$ and 4 pores (because θ_0^3 is a rather small quantity). In the case of $N = 12$ pores, Eq. (8) significantly underestimates the correction to the monoporate case, which can be seen by comparing the dashed line in Fig. 6 *d* with the numerically obtained results.

These discrepancies can be understood by examining the mean distance between the pores. In the case of N pores distributed equidistantly along the equator, the pores start to touch each other when $\theta_0 = \pi/N$. At this point, the entire geometry of the problem fundamentally changes, and the N individual pores merge into a single pore, forming an equatorial poral belt. Pollen grains with a ring-like aperture at the equator can indeed be found; e.g., in *Zamioculcas zamiifolia* and *Gonatopus angustus* in the Araceae family. Geometric aspects of the problem—other than the volume occupied by the pores—are not accounted for by Eq. (8), and the deviation of the critical volume from the monoporate case indicates an elastic interaction between the pores mediated by the exine between them. A physical explanation of this effect requires considerations of the pore packing on the grain surface, their mutual distance, and the total area they cover, which is a problem of characteristic lengths and areas rather than volumes. For our purposes, it is important to note that, for pore sizes typical for allergenic grains, $\theta_0 \sim 0.1$, the pores can be considered to be independent even when they are numerous because the critical volumes below $\theta_0 \approx 0.12$ are quite similar for $N = 1$ to 4 and even for $N = 12$. In this region, the predictions of Eq. (8) are essentially fulfilled.

DISCUSSION

The mechanical model of the pollen grain used in this study predicts that the pores deform significantly more than the exine as a pollen grain swells. The presence of pores relieves the stress on the exine and reduces it below the values it would attain were the pores not present (Fig. 5). At the same time, the pores are also the weak parts of the grain wall that are likely to rupture first when the grain reaches a certain level of hydration because they undergo rapid inflation at a critical relative additional volume of the grain. This pore bursting mechanism, where the pore bulges out and assumes a hemispherical shape just before rupture, has been observed in experiments (13,50) and is similar to one of the grain rupture mechanisms proposed by Matamoro-Vidal et al. (9) for pollen grains with a resistant exine and delicate intine, which, in our model, corresponds to low values of f. Another mechanism observed by Matamoro-Vidal et al. (9), swelling of the grain without pore or exine bursting and without significant bulging of the pore, is also included in our model and is typical for grains with rather small pores. The pores are less prone to bursting as they become smaller (Fig. 4), and because the critical volume of bursting is inversely proportional to θ_0 (Eq. (7), smaller pores do not undergo the bursting transition until the grain swells to a large extent. In this case, this also means that the exine becomes more strained and that it can break before the pores

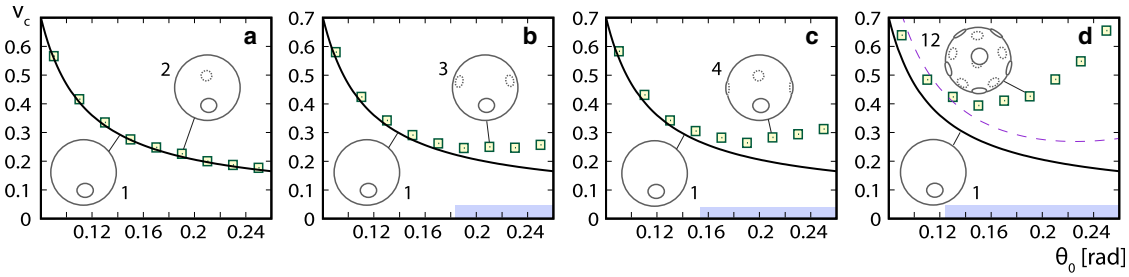

FIGURE 6 Critical volumes for grains with 1, 2, 3, 4 and 12 pores. Critical volume v_c for pollen grains with $f = 0.02$ and $\overline{\gamma} = 10^4$ as a function of pore opening angle θ_0 in grains with (*a*) $N = 2$, (*b*) 3, (*c*) 4, and (*d*) 12 pores. Numerical results are denoted by symbols, and full lines represent numerically obtained critical volumes of monoporate grains. The dashed line in (*d*) shows the results of Eq. (8) for $N = 12$. Thick light-blue lines above the x axes in (*b*)–(*d*) indicate the approximate regions of θ_0 in which the pores interact with each other. To see this figure in color, go online.

do. Fracture of the exine was also observed by Matamoro-Vidal et al. (9), but only in inaperturate pollen grains with a relatively thin exine. These observations and our model therefore suggest that the pores are, in general, indeed the weak spots of the grain and that they will—when present—typically rupture first. Although the calculated strains in the pores can become huge at the bursting transition (see, e.g., Fig. 2), where our assumption of Hookean elasticity (Eq. (1)) is likely to break down, the transition also survives in a more general, non-Hookean parametrization of the stretching energy (see the supporting material).

The critical volumes predicted by our model can be related to values observed in experiments. When the increase in mass of pollen grains was measured at different relative humidities (RHs) (20), it was found that until RH $\approx 85\%$ the grains absorb water internally, whereas for even larger values of RH, a water layer forms on the external surface of the grains. At RH $= 85\%$, the mass of pollen grains increases by about 50%, a number that does not appear to vary much between different pollen types (20). Maximal volume expansion of pollen grains in the atmosphere can thus roughly be estimated to be about $v \approx 0.5$, which is similar to the typical values of v_c obtained in our study. This suggest that our model covers the salient aspects of pollen grain swelling and provides a correct estimate of the characteristic energies involved. In particular, the model supports the observation that pollen grains in the atmosphere are in a critical environment where changes in humidity may easily lead to grain bursting, depending on the structure of the grains (11). Grains with sufficiently hard and small pores can sustain a large volume increase without their pores bursting. Although colpate pollen (pollen with elongated apertures) is not the subject of this work, it is nevertheless of interest to note that some colpate pollen (e.g., *Petunia hybrida*), can swell to a huge extent, increasing its volume two or three times upon hydration (40).

Diameters of pollen grains and the size of their pores show a significant correlation across different species of grasses (36,37), which suggests that their pore opening angles are approximately constant and can be estimated to be in the range of $\theta_0 \approx 0.06$ to 0.09 (at least in the grass species studied). Such a low value of θ_0 suggests that the pores of pollen grains of grasses are, interestingly, not particularly prone to bursting. This is partially confirmed by experiments (11) where it was found that, although 87% of *B. pendula* pollen grains release subpollen particles when hydrated for 10 min, only 40% of *P. pratense* pollen grains do so under the same conditions. The mean pore opening angle of monoporate grains of *P. pratense* (Fig. 1 *b*) can be estimated to be about $\theta_0 \approx 0.08$, whereas the pores of triporate pollen grains of *B. pendula* have a significantly larger opening angle of $\theta_0 \approx 0.13$ (3) (Fig. 1 *d*). This fact alone might explain the more frequent rupture of *Betula* pollen in a humid atmosphere.

On the other hand, such simple reasoning does not explain the fact that triporate pollen grains of *Parietaria judaica* with $\theta_0 \approx 0.09$ (3) burst five times less frequently than pollen grains of *P. pratense* even though they have similar pore opening angles. One should, however, keep in mind that the argument depends on the assumption of a similar value of aperture softness f, and different values of f can be expected in different pollen species (51), not only because of the differences in apertures and their thickness but also because of the differences in exine thickness and composition since f is a parameter that depends on the relative softness of the apertures. Although the values of f in porate pollen grains are in general unknown, it is nevertheless possible to estimate them in some cases. Rupture of pentoporate pollen grains of *U. parvifolia* has been recorded in a video sequence by Miguel et al. (13), and individual frames can be used to determine θ_0 and v_c because the volumes right before and after pore rupture can be determined from the sizes of the grain in different frames. This analysis gives $\theta_0 \approx 0.11$ and $v_c \approx 0.3$, which enables one to combine the two numbers and estimate the pore softness to be $f \approx 0.015$ (Fig. 4), in line with previous estimates (8,10).

Pore sizes in pollen of grasses appear to be particularly small, which could signify an evolutionary path that, on one hand, allows a soft spot in the grain to ease pollen tube growth and, on the other hand, maximally reduces its size to retain the mechanical consistency of the grain. The

minimal pore size is constrained by the size of the sperm cell, which has to pass through the pore into the pollen tube, and a comparison of typical sizes indeed suggests that the pores in grasses are maximally reduced. There also exist pollen grains with a number of quite large pores; for example, the pantoporate grains of *Gypsophila perfoliata* and *S. aquatica* (Fig. 1 *e*). Such an evolutionary solution enables accommodation of large additional volumes before one of the pores bursts. This is manifested by the characteristic shape of the dependence of v_c on θ_0 in Fig. 6 *d*, where v_c increases with θ_0 for sufficiently large pores. This shows that large critical volumes can be obtained not only by a single small pore but also by many large pores (θ_0>0.16 for the parameters used in Fig. 6). In this respect, it is interesting to note that pantoporate pollen grains appear to have evolved independently many times in different clades of flowering plants (52).

Thinning of the pollen wall in the form of an aperture enables efficient initiation of pollen tube growth but, at the same time, is a mechanical weakness of pollen grain. The same mechanical devices that would, under proper conditions, aid pollen tube germination can lead to grain rupture and the release of cytoplasm when the grain hydrates in an environment with inadequate osmolarity and ionic content, as might happen in the atmosphere. We have shown that the relative additional volume v_c, which can be sustained by a nearly spherical porate grain, and the potential of the grain to rupture are determined predominantly by the ratio f/θ_0 (Eq. (7)), a dimensionless parameter combining pore softness and its size. Other properties of the pollen grain, such as the number of pores, their precise distribution, and the contribution of bending in the process of bursting appear to be less important as long as the pores are sufficiently small.

SUPPORTING MATERIAL

Supporting material can be found online at https://doi.org/10.1016/j.bpj.2022.01.019.

AUTHOR CONTRIBUTIONS

A.Š. designed and performed the research. A.B. and A.Š. analyzed the data and wrote the paper.

ACKNOWLEDGMENTS

A.B. acknowledges funding from the Slovenian Research Agency ARRS (Research Core Funding No. P1–0055).

REFERENCES

1. Firon, N., M. Nepi, and E. Pacini. 2012. Water status and associated processes mark critical stages in pollen development and functioning. *Ann. Bot.* 109:1201–1213.
2. Hoekstra, F. A. 2002. Pollen and spores: desiccation tolerance in pollen and the spores of lower plants and fungi. *In* Desiccation and Survival in Plants: Drying without Dying. M. Black and H. W. Pritchard, eds. CAB International, pp. 185–205.
3. Halbritter, H., S. Ulrich, …, A. Frosch-Radivo. 2018. Illustrated Pollen Terminology. Springer.
4. Evert, R. F., and S. E. Eichhorn. 2013. Raven Biology of Plants. W. H. Freeman and Company.
5. Hamilton, E. S., G. S. Jensen, …, E. S. Haswell. 2015. Mechanosensitive channel MSL8 regulates osmotic forces during pollen hydration and germination. *Science.* 350:438–441.
6. Cameron, C., and A. Geitmann. 2018. Cell mechanics of pollen tube growth. *Curr. Opin. Genet. Dev.* 51:11–17.
7. Rakusová, H., and A. Geitmann. 2017. Pollen tip growth: control of cellular morphogenesis through intracellular trafficking. *In* Pollen Tip Growth. Springer, pp. 129–148.
8. Katifori, E., S. Alben, …, J. Dumais. 2010. Foldable structures and the natural design of pollen grains. *Proc. Natl. Acad. Sci. U S A.* 107:7635–7639.
9. Matamoro-Vidal, A., C. Raquin, …, P.-H. Gouyon. 2016. Links between morphology and function of the pollen wall: an experimental approach. *Bot. J. Linn. Soc.* 180:478–490.
10. Božič, A., and A. Šiber. 2020. Mechanical design of apertures and the infolding of pollen grain. *Proc. Natl. Acad. Sci. U S A.* 117:26600–26607.
11. Cecchi, L., E. Scala, …, R. Asero. 2020. Allergenicity at component level of subpollens particles from different sources obtained by osmolar shock: a molecular approach to thunderstorm-related asthma outbreaks. *Clin. Exp. Allergy.* 51:253–261.
12. Buters, J., M. Prank, …, L. Cecchi. 2015. Variation of the group 5 grass pollen allergen content of airborne pollen in relation to geographic location and time in season. *J. Allergy Clin. Immunol.* 136:87–95.
13. Miguel, A. G., P. E. Taylor, …, R. C. Flagan. 2006. Meteorological influences on respirable fragment release from Chinese Elm pollen. *Aerosol Sci. Technol.* 40:690–696.
14. D'Amato, G., G. Liccardi, and G. Frenguelli. 2007. Thunderstorm-asthma and pollen allergy. *Allergy.* 62:11–16.
15. M. Sofiev and K.-C. Bergmann, eds 2012. Allergenic Pollen: A Review of the Production, Release, Distribution and Health Impacts. Springer Science & Business Media.
16. Diethart, B., S. Sam, and M. Weber. 2007. Walls of allergenic pollen: special reference to the endexine. *Grana.* 46:164–175.
17. Shams, M., and S. Fineman. 2016. High Chinese elm pollen counts in the fall in Atlanta, Georgia, 2009–2015. *Ann. Allergy Asthma Immunol.* 117:553–554.
18. Diehl, K., C. Quick, …, R. Jaenicke. 2001. The ice nucleating ability of pollen. *Atmos. Res.* 58:75–87.
19. Pope, F. D. 2010. Pollen grains are efficient cloud condensation nuclei. *Environ. Res. Lett.* 5:044015.
20. Griffiths, P. T., J.-S. Borlace, …, F. D. Pope. 2012. Hygroscopic growth and cloud activation of pollen: a laboratory and modelling study. *Atmos. Sci. Lett.* 13:289–295.
21. Wozniak, M. C., F. Solmon, and A. L. Steiner. 2018. Pollen rupture and its impact on precipitation in clean continental conditions. *Geophys. Res. Lett.* 45:7156–7164.
22. Parre, E., and A. Geitmann. 2005. More than a leak sealant. The mechanical properties of callose in pollen tubes. *Plant Physiol.* 137:274–286.
23. Edlund, A. F., Q. Zheng, …, D. Preuss. 2016. Pollen from Arabidopsis thaliana and other Brassicaceae are functionally omniaperturate. *Am. J. Bot.* 103:1006–1019.
24. Wang, R., and A. A. Dobritsa. 2018. Exine and aperture patterns on the pollen surface: their formation and roles in plant reproduction. *In* Annual Plant Reviews Online. J. Roberts, ed. John Wiley & Sons, pp. 1–40.

25. Vieira, A. M., and J. A. Feijó. 2016. Hydrogel control of water uptake by pectins during in vitro pollen hydration of Eucalyptus globulus. *Am. J. Bot.* 103:437–451.

26. Ackerman, J. D. 2000. Abiotic pollen and pollination: ecological, functional, and evolutionary perspectives. *Plant Syst. Evol.* 222:167–185.

27. Seung, H. S., and D. R. Nelson. 1988. Defects in flexible membranes with crystalline order. *Phys. Rev. A Gen. Phys.* 38:1005–1018.

28. Lidmar, J., L. Mirny, and D. R. Nelson. 2003. Virus shapes and buckling transitions in spherical shells. *Phys. Rev. E.* 68:051910.

29. Gompper, G., and D. M. Kroll. 1996. Random surface discretizations and the renormalization of the bending rigidity. *J. Phys.* 6:1305–1320.

30. Hartmann, E. 1998. A marching method for the triangulation of surfaces. *Vis. Comput.* 14:95–108.

31. Šiber, A. 2020. Icosadeltahedral geometry of geodesic domes, fullerenes and viruses: a tutorial on the T-number. *Symmetry.* 12:556–1–556–22.

32. Hager, W. W., and H. Zhang. 2006. Algorithm 851: CG_DESCENT, a conjugate gradient method with guaranteed descent. *ACM Trans. Math. Softw.* 32:113–137.

33. Šiber, A. 2006. Buckling transition in icosahedral shells subjected to volume conservation constraint and pressure: relations to virus maturation. *Phys. Rev. E Stat. Nonlin Soft Matter Phys.* 73:061915.

34. Celik, G., D. Mungan, Z. Misirligil…, 2005. Poplar pollen-related allergy in Ankara, Turkey: how important for patients living in a city with high pollen load? *Allergy Asthma Proc.* 26:113–119.

35. Borsch, T. 1998. Pollen types in the Amaranthaceae. Morphology and evolutionary significance. *Grana.* 37:129–142.

36. Joly, C., L. Barillé, …, L. Visset. 2007. Grain and annulus diameter as criteria for distinguishing pollen grains of cereals from wild grasses. *Rev. Palaeobot. Palynol.* 146:221–233.

37. Jan, F., L. Schüler, and H. Behling. 2015. Trends of pollen grain size variation in C3 and C4 Poaceae species using pollen morphology for future assessment of grassland ecosystem dynamics. *Grana.* 54:129–145.

38. Wan, C., and J. Liu. 2017. The morphology and systematics of the pollen of Stellaria. *Palynology.* 41:1–14.

39. Haas, J., W. Creamer, …, C. V. Rodríguez. 2013. Evidence for maize (Zea mays) in the late archaic (3000–1800 B.C.) in the Norte Chico region of Peru. *Proc. Natl. Acad. Sci. U S A.* 110:4945–4949.

40. Gilissen, L. J. 1977. The influence of relative humidity on the swelling of pollen grains in vitro. *Planta.* 137:299–301.

41. Zuberi, M. I., and H. G. Dickinson. 1985. Pollen-stigma interaction in Brassica. III. Hydration of the pollen grains. *J. Cell Sci.* 76:321–336.

42. Šiber, A., and P. Ziherl. 2017. Cellular Patterns. CRC Press, Taylor & Francis Group.

43. Božič, A. L., and A. Šiber. 2018. Electrostatics-driven inflation of elastic icosahedral shells as a model for swelling of viruses. *Biophys. J.* 115:822–829.

44. Wang, Q., S. Nakamura, …, M. Miwa. 2012. Release behavior of small sized daughter allergens from Cryptomeria japonica pollen grains during urban rainfall event. *Aerobiologia.* 28:71–81.

45. Liu, T., and Z. Zhang. 2004. Mechanical properties of desiccated ragweed pollen grains determined by micromanipulation and theoretical modelling. *Biotechnol. Bioeng.* 85:770–775.

46. Wang, K., A. A. Abdala, …, M. K. Khraisheh. 2017. Mechanical characterization of membranes. *In* Membrane Characterization. N. Hilal, A. Ismail, and …, D. Oatley-Radcliffeeds. Elsevier, pp. 259–306, Chap. 13.

47. Suryanto, H., M. Muhajir, …, U. Yanuhar. 2019. The mechanical strength and morphology of bacterial cellulose films: the effect of NaOH concentration. *IOP Conf. Ser. Mater. Sci. Eng.* 515:012053-1–012053-7.

48. Bogen, D. K., and T. A. McMahon. 1979. Do cardiac aneurysms blow out? *Biophys. J.* 27:301–316.

49. Reuge, N., F. M. Schmidt, …, F. Abbé. 2001. Elastomer biaxial characterization using bubble inflation technique. I: experimental investigations. *Polym. Eng. Sci.* 41:522–531.

50. Taylor, P. E., R. C. Flagan, …, M. M. Glovsky. 2002. Release of allergens as respirable aerosols: a link between grass pollen and asthma. *J. Allergy Clin. Immunol.* 109:51–56.

51. Hargrove, L., and M. G. Simpson. 2003. Ultrastructure of heterocolpate pollen in Cryptantha (Boraginaceae). *Int. J. Plant Sci.* 164:137–151.

52. Prieu, C., H. Sauquet, …, B. Albert. 2017. More than sixty origins of pantoporate pollen in angiosperms. *Am. J. Bot.* 90:924–930.

Biophysical Journal, Volume *121*

Supplemental information

Mechanics of inactive swelling and bursting of porate pollen grains

Anže Božič and Antonio Šiber

SUPPORTING MATERIAL:
Mechanics of inactive swelling and bursting of porate pollen grains

Anže Božič
Department of Theoretical Physics, Jožef Stefan Institute, Jamova 39, 1000 Ljubljana, Slovenia

Antonio Šiber
Institute of Physics, Bijenička cesta 46, 10000 Zagreb, Croatia[*]
(Dated: January 13, 2022)

GENERATING CROSS-SECTIONAL PROJECTIONS OF MODEL POLLEN GRAINS

In Figs. 2 and 3 in the main text we show cross-sectional projections of the pollen grains. These are 2D projections of a 3D shape obtained by assuming rotational symmetry of the shape around the axis going through the geometric center of the shape and the pole of the pore. In the case of a single pore, the shape is indeed symmetric around this axis to an excellent accuracy, which can also be seen from the cross-sectional projections. The data shown in the figures was obtained by binning the face centers in 800 (2×400) angular intervals and calculating the average 2D-projected, cross-sectional coordinates in each of the intervals. The origin for such angular representation was positioned on the symmetry axis, at the point where the vertical line in the plots separates the pore from the exine. Such a procedure produces a set of data suitable for graphic representation.

ANALYTICAL APPROXIMATIONS FOR CRITICAL VOLUME AT BURSTING TRANSITION

A monoporate pollen grain with a relative additional volume v can be approximated as a union of two spherical caps: the first of radius R_{ex} representing the exine part of the grain, and the second of radius R_p representing the pore. Initially, $R_p = R_e$, but as v increases and the pore inflates, R_p continuously decreases all the way until the pore assumes the shape of a hemisphere, where R_p is the smallest. After this point, any further inflation of the pore requires an increase in R_p.

The internal pressure in the grain p is counteracted by the forces in the pollen wall. Examination of the force equilibrium in the two poles of the grain (one in the pore and the other in the exine) when the pore has a hemispherical shape yields

$$\frac{2T_p}{R_p} = \frac{2T_{ex}}{R_{ex}} = p, \tag{S1}$$

where T_p and T_{ex} are the tension stresses in the pore and the exine, respectively [1]. In the hemispherical state of the pore, we have $R_p = R_{ex}\theta_0$ and consequently $T_{ex} = T_p/\theta_0$. If the dominant contribution to the tension forces comes from the stretching part of the two-dimensional (2D) elastic energy, the stretching stresses T are proportional to strains ϵ, which gives

$$\epsilon_{ex} = \frac{f}{\theta_0}\,\epsilon_p, \tag{S2}$$

where we have accounted for the fact that the 2D stretching modulus of the pore is softer by a factor of f with respect to the corresponding 2D stretching modulus of the exine. The stretching strains can be obtained by examining the distances between the two points in the wall in the stress-free state of the grain and the corresponding distances in the inflated state of the grain, which gives

$$\begin{aligned} \epsilon_{ex} &= \frac{R_{ex}}{R_0} - 1, \\ \epsilon_p &= \frac{R_{ex}}{R_0}\,\frac{\pi}{2} - 1. \end{aligned} \tag{S3}$$

[*] asiber@ifs.hr

When $\theta_0 \ll 1$, the relative additional volume of the pollen grain with a hemispherical pore is given by

$$v_c = \left(\frac{R_{ex}}{R_0}\right)^3 \left(1 + \frac{\theta_0^3}{2}\right) - 1. \tag{S4}$$

From Eqs. (S2) and (S3), we have

$$\frac{R_{ex}}{R_0} = \frac{\theta_0 - f}{\theta_0 - f\pi/2}, \tag{S5}$$

and inserting Eq. (S5) into Eq. (S4), we obtain Eq. (6) in the main text. For a typical pollen grain, $f/\theta_0 \ll 1$ and $\theta_0 \ll 1$, and in this limit we further obtain Eq. (7) in the main text.

This derivation is only an approximation and is limited in scope. Equation (6) predicts that the bursting transition occurs only if $\theta_0 > f\pi/2$, as $v_c \to \infty$ when $\theta_0 = f\pi/2$. This is mostly satisfied by pollen grains, but it should be noted that the increase in volume in some pollen grains at bursting is comparable to the volume of a fully hydrated grain, $v \sim 1$. Furthermore, in the analytical derivation, the characteristic curvatures are assumed to be sphere-like, i.e., identical in the two principal directions both in the exine and in the pore. Numerically determined shapes do not have this property, although the principal curvatures do not differ much. The role of the neck region where the pore contacts the exine is also neglected in the approximation, even though it influences the curvatures of the grain shape, even in the polar region of the pore. This is particularly important for larger values of the softness parameter when the approximation of sphere-like curvatures becomes less accurate.

Validity of analytical approximations for bursting transition

While the numerical results presented in the main text mostly account for the geometry and elastic inhomogeneity which are to be expected in porate pollen grains (parameters θ_0 and f), it is of interest to examine the bursting transition for a wider range of parameters, since the bursting transition should vanish once the pore becomes hard enough. This will certainly be the case when $f = 1$ and the grain becomes effectively inaperturate, with $v_c \to \infty$. The analytical model in Eq. (6), however, predicts a divergence of v_c when $f = 2\theta_0/\pi$. In Fig. S1, we show how v_c changes as a function of f for a fixed $\theta_0 = 0.15$. Though large values of f (i.e., $f > 0.05$) are not expected to be typical for pollen grains [2, 3], the investigation of grains with larger f is nevertheless important in the more general context of the mechanics of soft pore inflation. The results indicate that the analytical approximation serves as a reasonably accurate guideline when $v_c < 0.8$, which is a situation typically encountered in pollen swelling and bursting. The approximations become significantly less reliable when $v_c > 1$. Somewhat fortuitously, the functional dependence in Eq. (7) can be used as a lower bound estimate for all the volumes v_c studied.

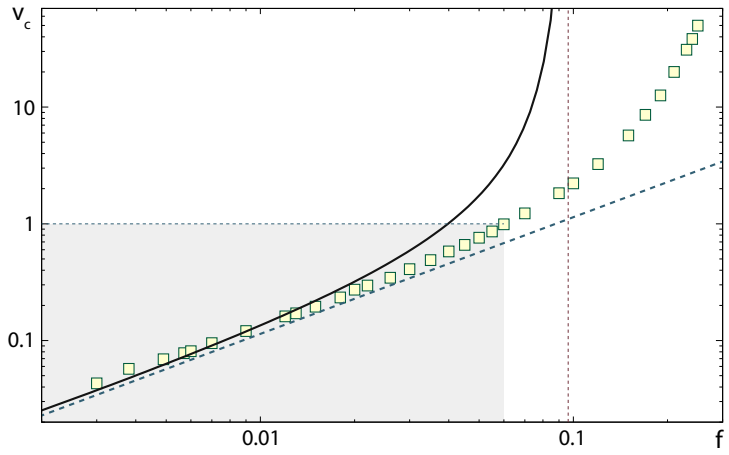

Figure S1. Critical volume at bursting transition v_c for a monoporate pollen grain with $\theta_0 = 0.15$ and $\overline{\gamma} = 10^4$ as a function of the pore softness parameter f. Numerically obtained results are denoted by symbols. Full and dashed lines are the predictions of Eq. (6) and Eq. (7) in the main text, respectively. The thin vertical dashed line indicates the value of f where the analytical expression in Eq. (6) diverges, $f = 2\theta_0/\pi$. The gray area of the plot indicates the range of (f, v_c) parameter space relevant to most pollen grains.

INTERNAL PRESSURE AND BURSTING TRANSITION

The calculations in the main text were performed for a given relative additional volume of the grain v. To each of the grain states obtained with the volume constraint one can also attribute an internal pressure P. The internal pressure can be obtained from the normal forces acting on the vertices of the shell in the absence of the volume constraint [4]. Figure S2 shows how the internal pressure in the pollen grain changes as its volume increases—this calculation is performed for the same set of parameters as those used in Fig. 2 in the main text. A sufficient pressure, denoted by P_c in Fig. S2, is required to overcome the energy barrier for bursting and the pressure drops once the pore inflates. This is similar to the phenomena observed in the inflation of a circular membrane [5] and rubber balloons [6, 7]. Comparing these results with those obtained by Božič and Šiber [4] for thin homogeneous spherical shells, we observe that the values of pressure are quite similar at a given increase of volume or exine radius. The pore decreases the pressure in the grain below the pressure which would act in an inaperturate grain at the same relative additional volume. This is indicated by the dashed line in Fig. S2, which shows the pressure obtained in the analytical limit of the microscopic model in Eq. (1) in the main text for an inaperturate grain with the stretching contribution only, $P = 2k_{ex}/(\sqrt{3}R_0)\, v$ [4].

We have also performed elastic energy minimization at a fixed internal pressure instead of the grain volume. In this case, the energy functional is augmented by an addition of a term PV [4, 8], and the volume constraint is released—this approach can be of interest when grain swelling is studied in solutions with different concentrations of non-metabolic sugars [9]. The calculations perfectly reproduce the critical volumes obtained in the fixed volume calculations, but the shapes obtained after the bursting transition (for $P > P_c$) have very large volumes and are difficult to stabilize in the minimization procedure. The large volumes of these shapes could also have been guessed on the basis of the nature of the pressure dependence in Fig. S2—the pressure *decreases* for $v > v_c$, which means that it can eventually return to its critical value of P_c only for large values of relative additional volume v. The bursting transition thus figures much more prominently in the calculations at a fixed internal pressure, although the grain shapes after the transition are difficult to obtain. Both approaches strongly corroborate the necessity of bursting (rupture) of the pore at $P = P_c$ or $v = v_c$ ($P_c = 0.232\ k/R_0$ and $v_c = 0.26$ for the case shown in Fig. S2 and Fig. 2, respectively).

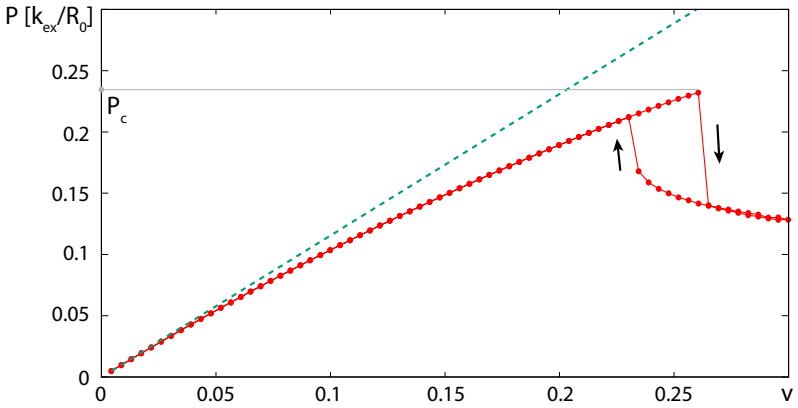

Figure S2. Internal pressure in the grain P as a function of the relative additional volume v. The pressure is shown in reduced dimensionless units of k_{ex}/R_0. Numerically obtained results are denoted by symbols. The dashed line shows the pressure obtained in the analytical limit of the microscopic model for the homogeneous inaperturate shell with stretching energy contribution only, $P = 2k_{ex}/(\sqrt{3}R_0)\, v$. The forward and backward minimization paths are indicated by arrows. The parameters of the calculation are the same as in Fig. 2 in the main text, $f = 0.02$, $\theta_0 = 0.15$, and $\overline{\gamma} = 10^4$.

INFLUENCE OF BENDING ENERGY ON BURSTING TRANSITION

All the results shown in the main text are calculated for $\overline{\gamma} = 10^4$. The range of $\overline{\gamma}$ typical for pollen grains was estimated by Božič and Šiber [2] to be between 3000 and 10000. This interval of $\overline{\gamma}$ was obtained by requiring that the colpate grains close regularly and completely as they dry up, and might not be entirely relevant for porate grains studied in this work. It is of interest to examine how different values of $\overline{\gamma}$ influence the bursting transition. Figure S3 shows how the critical volume at the bursting transition depends on the pore opening angle for three different values of $\overline{\gamma}$; smaller values of $\overline{\gamma}$ indicate a larger contribution of the bending energy. Figure S3 demonstrates that although

the bending energy influences the critical volumes (and pressures), the influence is relatively small and the results obtained in the main text for $\overline{\gamma} = 10^4$ can be considered to be representative for pollen grains. The bursting transition is smoother for smaller $\overline{\gamma}$, so that the full expansion of the pore occurs in a wider interval of volume.

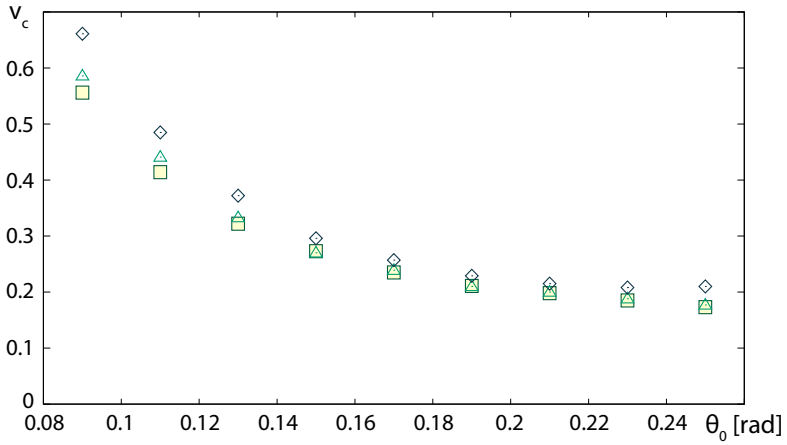

Figure S3. Critical volume at bursting transition v_c as a function of the pore opening angle θ_0 for $\overline{\gamma} = 10^4$ (squares), 5×10^3 (triangles), and 10^3 (diamonds). The pore softness parameter is $f = 0.02$.

NONLINEAR STRESS-STRAIN DEPENDENCE AND (NON-)UNIVERSALITY OF BURSTING TRANSITION

The calculated strains in the pore can become huge at the bursting transition. For instance, in the example in Fig. 2, the maximal extensional strain of the pore material *at* the bursting transition is 2.6. Such huge strains may require a modification of the Hookean stress-strain relationship employed in our simulations (see Materials and Methods in the main text). While such modifications can in principle be included in our model by allowing the elastic constants to vary with the local strain, in the situation where the elastic responses of the exine and the intine are poorly known such an undertaking does not appear to be particularly enlightening. Nevertheless, it is important to examine the robustness of the predicted bursting transition and investigate whether it persists in different elastic models of the pollen grain. To this end, we modified the stretching part of the Hookean elastic energy [Eq. (1)] to read

$$E_{stretch} = \sum_i \frac{k_i l_{i,0}^2}{2} \left| \frac{l_i}{l_{i,0}} - 1 \right|^p , \tag{S6}$$

where p is a real number, and performed calculations analogous to those shown in Fig. 2 (which correspond to the Hookean elasticity where $p = 2$). The formulation in Eq. (S6) has the advantage that the microscopic stretching and bending elastic constants of the edges k_i and ρ_i are kept the same for all p and have the same units as in the Hookean case. The stretching energies of the Hookean case and the p-power stretching elasticity coincide in an edge of length $l_i/l_{i,0} = 2$.

The pore bursting transition survives also in the more general parametrization of the stretching energy of Eq. (S6) for a range of values of p. There are, however, some differences from the Hookean case with $p = 2$. In particular, while the pores are visibly bulged out at the bursting transition for all powers p studied, the shape of the pore at the transition point is inflated a bit over the hemispherical shape when $p > 2$. Furthermore, the critical volumes of the transition sensitively depend on the power p, as demonstrated in Fig. S4. For $p > 2.4$, $v_c \gtrsim 1$ and the calculations become somewhat irrelevant for most porate grains as they do not tend to swell to such a high degree. It is also possible that for sufficiently large p, the bursting transition becomes completely suppressed and never takes place even for infinite increase in volume. This means that the aperture does not importantly modify the strains in the exine and that the entire grain swells almost as if it were inaperturate; this time not because the pore would be too small but due to the high power p in the nonlinear stress-strain relationship. A somewhat similar effect has been noted in relation to the blowout phenomenon of circular membranes and spherical patches, which takes place only for sufficiently small powers p in the energy functional of the problem [5]. A faithful modelling of pollen grain elasticity would require different parametrizations of the elasticity of the exine and the pores, in a much more involved manner

than using a simple scaling through a softness constant f. This is particularly relevant for large extensions of the exine and the pores, which are likely to be governed by quite different energy functionals and by an effective superposition of several power laws with different values of p [10].

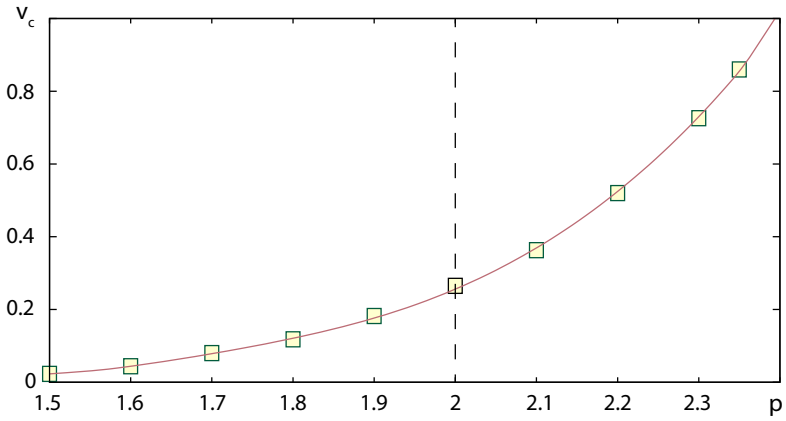

Figure S4. Critical volume v_c at which a pore rapidly inflates as a function of the power p in the parametrization of the stretching energy in Eq. (S6). Dashed vertical line emphasizes the point with $p = 2$ (Hookean dependence). The full line is a guide to the eye. The parameters of the elasticity of the monoporate grain are $f = 0.02$, $\theta_0 = 0.15$, and $\overline{\gamma} = 10^4$.

CODE AVAILABILITY

The computational code used to obtain the numerical results in the manuscript and the files pertaining to it (input files and the README file with the instructions required to reproduce the calculations) are publicly available in their entirety through the Open Science Framework (OSF): `https://osf.io/4q9ya/` [11].

[1] A. Šiber and P. Ziherl, *Cellular Patterns* (CRC Press, Taylor & Francis Group, Boca Raton, 2017).
[2] A. Božič and A. Šiber, Mechanical design of apertures and the infolding of pollen grain, Proc. Natl. Acad. Sci. USA **117**, 26600 (2020).
[3] E. Katifori, S. Alben, E. Cerda, D. R. Nelson, and J. Dumais, Foldable structures and the natural design of pollen grains, Proc. Natl. Acad. Sci. USA **107**, 7635 (2010).
[4] A. L. Božič and A. Šiber, Electrostatics-driven inflation of elastic icosahedral shells as a model for swelling of viruses, Biophys. J. **115**, 822 (2018).
[5] D. K. Bogen and T. A. McMahon, Do cardiac aneurysms blow out?, Biophys. J. **27**, 301 (1979).
[6] H. Alexander, Tensile instability of initially spherical balloons, Int. J. Eng. Sci. **9**, 151 (1971).
[7] A. Needleman, Inflation of spherical rubber balloons, Int. J. Solids Structures. **13**, 409 (1977).
[8] A. Šiber, Buckling transition in icosahedral shells subjected to volume conservation constraint and pressure: Relations to virus maturation, Phys. Rev. E **73**, 061915 (2006).
[9] A. Matamoro-Vidal, C. Raquin, F. Brisset, H. Colas, c. B. Iza, B. Albert, and P.-H. Gouyon, Links between morphology and function of the pollen wall: An experimental approach, Bot. J. Linn. Soc. **180**, 478 (2016).
[10] R. Ogden, Large deformation isotropic elasticity – on the correlation of theory and experiment for incompressible rubberlike solids, Proc. R. Soc. Lond. A **326**, 565 (1972).
[11] A. Šiber and A. Božič, Swelling of porate pollen grains (2022), OSF, 12 Jan. 2022. `https://osf.io/4q9ya`.